HEALTH AND MEDICINE

Retinoid X receptor alpha is a spatiotemporally predominant therapeutic target for anthracycline-induced cardiotoxicity

Xiao Ma[1,2,3,4], Ping Zhu[1,2], Yonghe Ding[1,2], Hong Zhang[1,2,5], Qi Qiu[1,2,6], Alexey V. Dvornikov[1,2], Zheng Wang[7], Maengjo Kim[1,2], Yong Wang[1,2,8], Matthew Lowerison[9], Yue Yu[10], Nadine Norton[11], Joerg Herrmann[2], Stephen C. Ekker[1,3,4], Tzung K. Hsiai[12], Xueying Lin[1,2], Xiaolei Xu[1,2,3,4]*

To uncover the genetic basis of anthracycline-induced cardiotoxicity (AIC), we recently established a genetic suppressor screening strategy in zebrafish. Here, we report the molecular and cellular nature of *GBT0419*, a salutary modifier mutant that affects *retinoid x receptor alpha a (rxraa)*. We showed that endothelial, but not myocardial or epicardial, *RXRA* activation confers AIC protection. We then identified isotretinoin and bexarotene, two FDA-approved RXRA agonists, which exert cardioprotective effects. The therapeutic effects of these drugs only occur when administered during early, but not late, phase of AIC or as pretreatment. Mechanistically, these spatially- and temporally-predominant benefits of *RXRA* activation can be ascribed to repair of damaged endothelial cell-barrier via regulating tight-junction protein Zonula occludens-1. Together, our study provides the first in vivo genetic evidence supporting *RXRA* as the therapeutic target for AIC, and uncovers a previously unrecognized spatiotemporally-predominant mechanism that shall inform future translational efforts.

INTRODUCTION

Anthracycline is a group of chemotherapeutic drugs that are being actively used to treat broad types of cancer (*1*, *2*), but the major clinical complication for these antibiotics is their dose-dependent cardiotoxicity (*1*). Several mechanisms have been proposed for anthracycline-induced cardiotoxicity (AIC), including topoisomerase IIβ (coded by *TOP2B*) as a primary mediator (*3*). On the basis of these mechanisms, dexrazoxane, an iron chelator, has been successfully developed as the only U.S. Food and Drug Administration (FDA)–approved AIC preventive compound. Nevertheless, late-onset decompensated cardiomyopathies remain life-threatening for patients with AIC, as approximately 50% of patients die 2 years after diagnosis (*4*), which calls for more mechanistic studies and therapeutic developments. While cardiomyocytes have long been perceived as the primarily affected cellular target, recent evidence has indicated that the abnormalities in noncardiomyocytes, including endothelial cells (*5*), vascular smooth muscle cells (*6*), and cardiac fibroblasts (*7*, *8*), also contribute notably to AIC pathogenesis. Therapeutic strategies based on these noncardiomyocytes, however, remain underexplored.

To elucidate the disease mechanisms and to search for potential therapeutic targets, several genetic strategies, such as genome-wide association study (GWAS), have been recently used to identify genetic modifiers that affect the onset and severity of AIC. The completion of two large-scale human genetic studies revealed rs2229774 [*retinoic acid receptor* γ (*RARG*)] and rs28714259 (intergenic region) as two susceptible variants to AIC (*9*, *10*). Through a GWAS analysis of decline in left ventricular ejection fraction (EF) in 1191 patients with early-stage breast cancer treated with doxorubicin (DOX) and trastuzumab, we also identified six putative loci for AIC (*11*). Nevertheless, because of its statistical nature, extensive experimental verifications are still needed to determine whether these affected genes are truly AIC modifiers and which genes can be leveraged for therapeutic benefits. Therefore, as a complementary strategy, we recently developed a zebrafish AIC model via injection of DOX (*12*) and established an in vivo screening platform to search for potential AIC modifying genes in a forward genetic manner (*13*). The screening is based on a collection of gene-break transposon (GBT) mutants (*14*), which are caused by the insertion of *pGBT-RP2* (RP2) elements containing both a protein trap and a polyadenylation (polyA) signal trap. Different from human genetic approaches, identities of genetic modifiers can be unambiguously uncovered, and mutants that exert salutary effects on AIC directly suggest therapeutic targets. Because of the integration of *loxP* sites in the RP2 vector, the mutated locus in each GBT mutant can be reverted conditionally (*15*). Thus, another unique, but yet to be realized, advantage of this zebrafish-based genetic screening is the feasibility of rapidly assigning modifying effects to the precise cell lineage(s), including both cardiomyocytes and noncardiomyocytes.

GBT0419 is the first salutary modifier identified from a pilot screening of 609 GBT lines (*13*), which exerts a long-term benefit on the survival of AIC adult zebrafish. In this mutant, the RP2 element is inserted within *retinoid X receptor alpha a* (*rxraa*), a zebrafish ortholog of human *retinoid X receptor alpha* (*RXRA*). In the cell nucleus, the RXRA protein is known to function as one of the primary receptors for retinoic acid (RA), which transcriptionally regulates a spectrum of biological processes such as embryogenesis, hemostasis, and xenoprotection (*16*). During embryonic stages, *RXRA* is

[1]Department of Biochemistry and Molecular Biology, Mayo Clinic, Rochester, MN, USA. [2]Department of Cardiovascular Medicine, Mayo Clinic, Rochester, MN, USA. [3]Center for Clinical and Translational Science, Mayo Clinic, Rochester, MN, USA. [4]Mayo Graduate School of Biomedical Sciences, Mayo Clinic, Rochester, MN, USA. [5]Clinical Center for Gene Diagnosis and Therapy, The Second Xiangya Hospital of Central South University, Changsha, China. [6]Institute of Clinical Pharmacology, Beijing Anzhen Hospital, Capital Medical University, Beijing, China. [7]Department of Medicine, Mayo Clinic, Rochester, MN, USA. [8]Institute of Life Science, Beijing University of Chinese Medicine, Beijing, China. [9]Department of Urology, Mayo Clinic, Rochester, MN, USA. [10]Department of Health Sciences Research, Mayo Clinic, Rochester, MN, USA. [11]Department of Cancer Biology, Mayo Clinic, Jacksonville, FL, USA. [12]School of Medicine, University of California, Los Angeles, Los Angeles, CA, USA.
*Corresponding author. Email: xu.xiaolei@mayo.edu

indispensable for cardiac morphogenesis, as *Rxra*-null mice do not survive because of heart failure resulting from the thinned myocardial compact zone (*17*). Cell lineage–specific presence of *RXRA* has been demonstrated to be critical in this process, as *RXRA* in epicardium, but not in myocardium or other cell lineages, appears to be exclusively required for normal heart development (*18*–*21*). During postnatal stages, abnormal expression of *RXRA* has been noted in failing hearts (*22*), and modulating *RXRA* with agonists has been recently shown to have cardioprotective effects (*23*). However, the potential cell lineage–specific roles of *RXRA* have not been systematically investigated in AIC or any other chronic pathological conditions.

Here, we conducted comprehensive genetic and pharmacological studies to elucidate the mechanisms underlying the salutary effects of *GBT0419*. In particular, we scanned the contributions of different cardiac cell lineages to *RXRA*-associated cardioprotection via conditionally reverting *GBT0419* in the endothelium, myocardium, and epicardium, which prompted a series of follow-up genetic studies to show that endothelial-specific *RXRA* gain of function is therapeutic for AIC. To translate this discovery, we identified two FDA-approved RXRA agonists and demonstrated that these drugs should be administered during the early phase of AIC, but not the late phase or as pretreatment, to maximize their therapeutic potential. Mechanistically, we ascribed the cardioprotective effects of *RXRA* activation, at least in part, to the restoration of impaired endothelial barrier function during early AIC progression. In summary, by identifying endothelial *RXRA* as a previously unrecognized therapeutic target, we demonstrated the necessity of an unbiased assessment of cell lineage–specific contribution for each previously unidentified AIC genetic factor and presented adult zebrafish as a highly efficient vertebrate model for this purpose.

RESULTS

Supporting GWAS evidence for *RXRA* as a genetic factor for AIC

To seek human relevance of *RXRA*, we searched our recent GWAS data of 1191 patients with early-stage breast cancer treated with DOX (*11*) and identified two common variants at the *RXRA* locus, rs11185662 and rs62576342 (European minor allele frequencies 0.24 and 0.45), which were associated with a decline in left ventricular EF, $P = 0.0006$ ($\beta = -3.359$) and $P = 0.001$ ($\beta = -3.466$), respectively (table S1). This human genetic evidence supports *RXRA* as a susceptibility gene for AIC and justifies the necessity to further characterize the functions of *RXRA* orthologs in zebrafish.

Endothelial-specific cardiac reversion of the RP2 insertion abolishes the salutary effects of *GBT0419* on AIC

In zebrafish, there are two orthologs for *RXRA*: *rxraa* and *rxrab*. Both genes encode highly conserved peptides to human RXRA, as indicated by >80% sequence similarity (fig. S1A). The cardiac expression of the *rxraa* transcript is 3.4 times higher than that of *rxrab* in embryos and 4.0 times higher in adults as revealed by a transcriptome analysis (Gene Expression Omnibus no. GSE85416 and data not shown), suggesting that *rxraa* is the dominant *RXRA* ortholog in a zebrafish heart. The expression of *rxraa* in adult zebrafish cardiac tissues was also confirmed by semiquantitative polymerase chain reaction (PCR) (fig. S1B).

Because a monomeric red fluorescent protein (mRFP), which is implanted in the RP2 vector, fuses in frame with the N-terminal part of the trapped gene in each GBT line (*14*), the fluorescence can be used to evaluate the endogenous gene expression pattern (*24*). We then characterized the mRFP pattern in *GBT0419* that contains the RP2 insertion in the first intron of *rxraa* (fig. S2A) and observed ubiquitous mRFP expression in the heart. To further define *rxraa* cardiac expression at a lineage resolution, we bred *GBT0419/0419* into *Tg(fli1a:EGFP)* to label endothelial cells and *Tg(ttn:actn-EGFP)* to label cardiomyocytes. Colocalization of $mRFP^+$ cells, which represents endogenous *rxraa* expression, with enhanced green fluorescent protein ($EGFP^+$) cells was noted in both double-transgenic backgrounds in the hearts at 6 days postfertilization (dpf) (fig. S2, B and C; global endothelial expression in fig. S1C), indicating that *rxraa* is expressed in cardiomyocytes, endothelial cells, and potentially other cardiac lineages.

To assess the cardiac contribution underlying the *GBT0419*-associated salutary effects, *GBT0419/0419* was bred into *Tg(kdrl:CreER)*, *Tg(cmlc2:CreER)*, and *Tg(tcf21:CreER)* to revert the RP2 insertion in the three cardiac lineages: endothelium, myocardium, and epicardium (Fig. 1A). Two triple-transgenic lines, *Tg(fli1a:EGFP);Tg(kdrl:CreER);GBT0419/0419* and *Tg(ttn:actn-EGFP);Tg(cmlc2:CreER);GBT0419/0419*, were generated to assess CreER-*loxP* efficacy. Treatment of embryos with 4-hydroxytamoxifen (4HT) from 0 to 6 dpf effectively removed the RP2 insertion in a lineage-specific manner (fig. S2, D and E), as indicated by the absence of mRFP fluorescence in either endothelial cells or cardiomyocytes.

The three *CreER*-based double-transgenic embryos (Fig. 1A) were then treated with either 4HT (to induce RP2 reversion) or ethanol (as a control), raised to up to 3 months of age (fig. S3A), stressed with DOX, and assessed for the consequences of RP2 lineage-specific reversion in three ways. First, we assessed survival of the fish after DOX stress over a 10-week period. While a reduction in DOX-induced death was observed in *GBT0419/0419* fish, the reversion of RP2 in endothelial cells, but not in myocardial or epicardial cells, diminished the survival benefit (Fig. 1, B, E, and F). Second, we assessed cardiac function using an ex vivo Langendorff-like system (*25*). While a reduced ventricular EF was noted in the wild-type fish at 10 weeks post–DOX injection (wpi) (48.2 ± 8.9% versus 57.3 ± 4.2%; $P = 0.002$), ventricular pump function was preserved in *GBT0419/0419* (fig. S3B). Consistent with the survival indices, the reversion of RP2 in endothelial cells, but not in myocardial or epicardial cells, attenuated this cardioprotective effect (Fig. 1C and fig. S3, D and E). Third, we quantified exercise capacity, a widely used clinical index for patients with heart failure. A gradual reduction in critical swimming speed (U_{crit}) was observed in adult fish with AIC at 4 wpi and thereafter (fig. S3C), and a preserved U_{crit} index was noted in *GBT0419/0419* even at 10 wpi (25.85 ± 5.53 versus 25.27 ± 4.87 body length/s; $P = 0.9000$). This preserved swimming capacity was abolished by endothelial-specific removal of the RP2 insertion (Fig. 1D). Collectively, these unbiased genetic analyses proved the cardiac contribution of the salutary modifying effects of *GBT0419* and further indicated that the molecular alteration of *rxraa* in endothelial cells, but not cardiomyocytes or epicardial cells, plays a more predominant role.

The cardioprotective effects of *GBT0419* are conferred by RA signaling activation

To define the molecular alteration in *GBT0419*, we generated $rxraa^{e2}$, a transcription activator–like effector nuclease (TALEN) mutant that harbors an eight-nucleotide deletion in the exon immediately following RP2 insertion in *GBT0419* (Fig. 2A). Because the indel

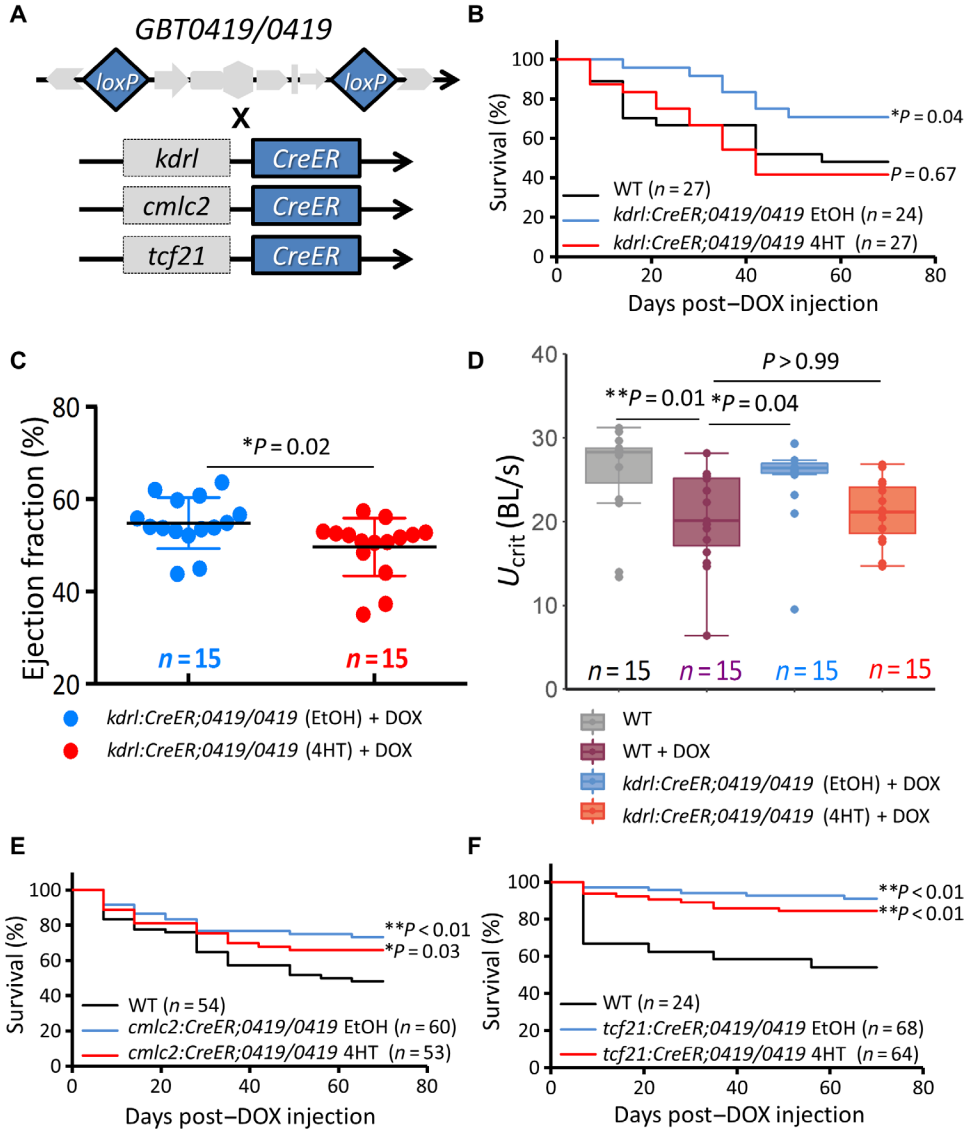

Fig. 1. Endothelial RP2 reversion in *GBT0419/0419* abolishes its cardioprotective effects on AIC. (**A**) The schematic shows the *Tg(kdrl:CreER)*, *Tg(cmlc2:CreER)*, and *Tg(tcf21:CreER)* transgenic lines that were crossed into *GBT0419/0419*, respectively. *CreER* and *loxP* elements are highlighted in blue. (**B**) Kaplan-Meier survival curves indicate reduced survival of *GBT0419/0419* adult fish with endothelial RP2 reversion after DOX stress. (**C**) The ventricular EF of *GBT0419/0419* adult fish was reduced with endothelial RP2 reversion after DOX stress. Each dot represents the EF value of a single ventricle. WT, wild type; EtOH, ethanol. (**D**) Swimming capacity of *GBT0419/0419* adult fish remains reduced with endothelial RP2 reversion after DOX stress. BL, body length; U_{crit}, critical swimming speed. (**E**) Kaplan-Meier survival curves indicate unchanged survival of *GBT0419/0419* adult fish with myocardial RP2 reversion after DOX stress. (**F**) Kaplan-Meier survival curves indicate unchanged survival of *GBT0419/0419* adult fish with epicardial RP2 reversion after DOX stress. Error bars represent SD. *$P < 0.05$ and **$P < 0.01$; log-rank test in (B), (E), and (F) for comparison with the WT group; unpaired Student's *t* test in (C); Kruskal-Wallis test was used followed by Tukey's post hoc test in (D).

presumably leads to a frameshift and a truncated Rxraa protein, *rxraa*^{e2} is likely a loss-of-function mutant (fig. S4, A to C). Unexpectedly, in contrast to the salutary modifying effects of *GBT0419/0419*, *rxraa*$^{e2/e2}$ worsened the fish survival (Fig. 2B), increased the apoptotic index at 8 wpi (Fig. 2, C and D), and failed to rescue declined cardiac functions in the AIC model (Fig. 2E and fig. S4, E to G). We measured the expression of two pathological markers for cardiac remodeling, *natriuretic peptide A* (*nppa*) and *natriuretic peptide B* (*nppb*) (Fig. 2, F and G), and detected the induction of *nppa* in *rxraa*$^{e2/e2}$ but not in *GBT0419/0419*. In contrast to the improved myofibril organization in *GBT0419/0419* at 12 wpi, which can be characterized by more even distribution of α-actinin, improved lateral alignment, and better-organized sarcomeres, the myofibrils remained disorganized in *rxraa*$^{e2/e2}$ (Fig. 2H).

Next, we compared the molecular alteration between *GBT0419* and *rxraa*^{e2}. While the RP2 insertion disrupted the splicing event between exon 1 and exon 2 with >90% efficacy (Fig. 3, A and B), *rxraa* transcripts after exon 2 were induced in *GBT0419/0419* (Fig. 3, A and C), potentially because of the strong enhancer/promoter in the RP2 vector. In contrast, the expression of *rxraa* transcript in *rxraa*$^{e2/e2}$ was reduced by ~50% (Fig. 3, B and C), presumably due to the nonsense-mediated mRNA decay. Of note, an in-frame methionine is

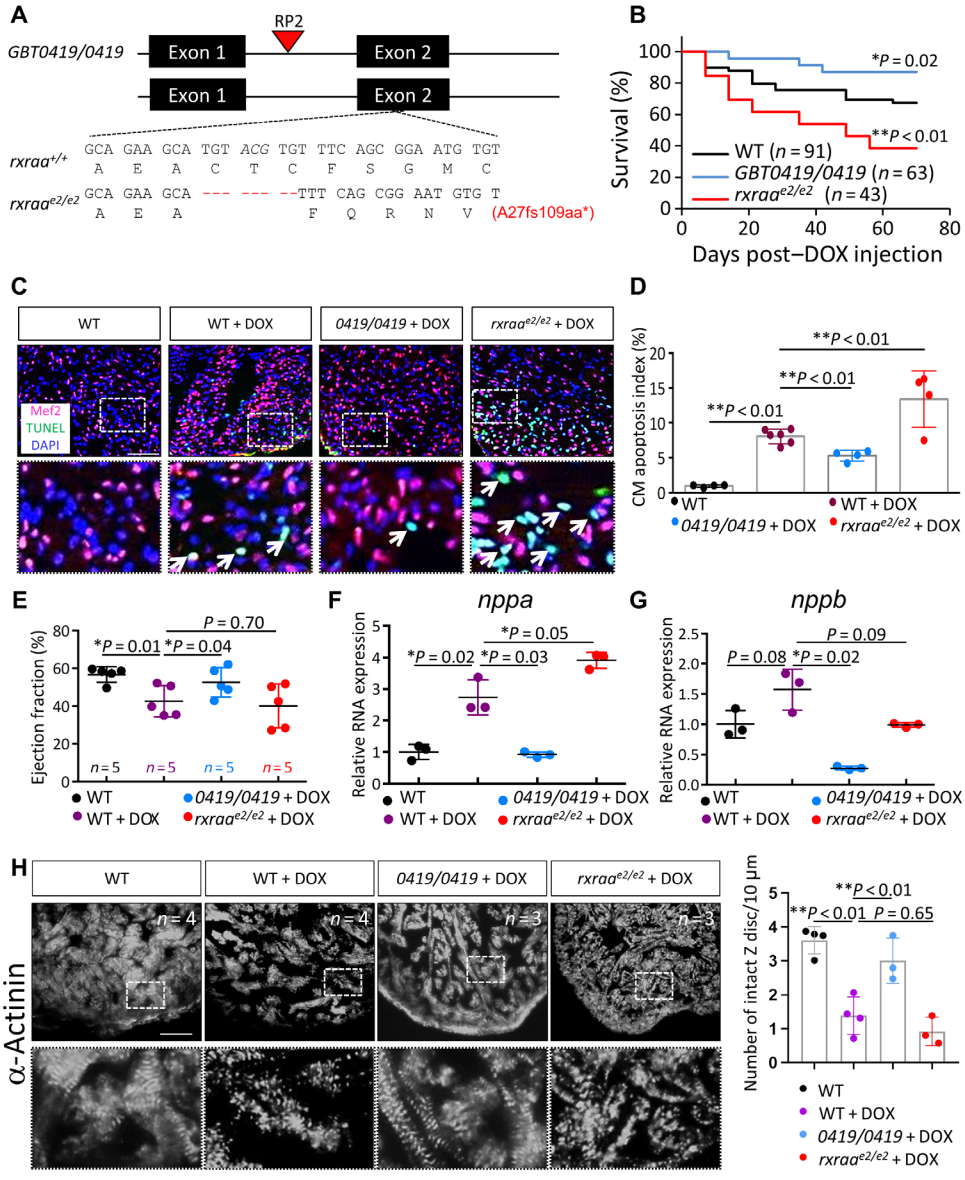

Fig. 2. While *GBT0419* exerts salutary effects, an *rxraa* TALEN allele exerts deleterious effects on AIC in adult zebrafish. (**A**) Schematic comparison of genomic lesions in *GBT0419/0419* and an *rxraa* TALEN mutant (*rxraa*$^{e2/e2}$). Dashed lines indicate an eight-nucleotide deletion. fs, frameshift; aa, amino acid. (**B**) Kaplan-Meier survival curves show survival of WT, *GBT0419/0419*, and *rxraa*$^{e2/e2}$ adult fish after DOX stress. (**C**) Representative images of cardiomyocyte apoptosis in the ventricular tissues of WT, *GBT0419/0419*, and *rxraa*$^{e2/e2}$ after DOX stress at 10 wpi. The bottom panels show a higher-magnification view of the corresponding dotted box area. Arrows indicate cardiomyocytes (Mef2^{+}) with positive terminal deoxynucleotidyl transferase–mediated deoxyuridine triphosphate nick end labeling (TUNEL) staining. Mef2, myocyte enhancer factor 2; DAPI, 4′,6-diamidino-2-phenylindole. Scale bar, 50 μm. (**D**) Quantification of the cardiomyocyte apoptosis index in (C). Each dot represents a single fish ventricle. Approximately 500 to 1000 cardiomyocytes were counted in sections per ventricle. CM, cardiomyocyte. (**E**) Ventricular EF of WT, *GBT0419/0419*, and *rxraa*$^{e2/e2}$ after DOX stress at 10 wpi. (**F** and **G**) The expression of *nppa* (F) and *nppb* (G) transcripts in WT, *GBT0419/0419*, and *rxraa*$^{e2/e2}$ after DOX stress at 10 wpi is shown. RNA was extracted from a pool of three ventricles as a single biological replicate. $n = 3$ in each group. (**H**) Images of α-actinin antibody staining show myofibril disarray in ventricular tissues of WT, *GBT0419/0419*, and *rxraa*$^{e2/e2}$ after DOX stress at 12 wpi. Bottom panels are higher-magnification views of the dotted box areas. $n > 3$ for each group. Quantification on the right shows the number of intact Z disc/10 μm. Scale bar, 50 μm. Error bars represent SD. *$P < 0.05$ and **$P < 0.01$; log-rank test in (B) for comparisons with the WT group; one-way analysis of variance (ANOVA) followed by Tukey's post hoc test in (D) to (G).

encoded within the second exon, which might serve as an alternative translation start site (fig. S1A), raising the possibility that *GBT0419* is a gain-of-function mutant. We then quantified the mRNA levels of several well-known RA-targeted genes (*26*) and found that most of these genes were substantially induced in *GBT0419/0419* at 2 dpf but remained inhibited or unchanged in *rxraa*$^{e2/e2}$ (Fig. 3D). Together, these data suggested that, in contrast to *rxraa*$^{e2/e2}$, RA signaling was net activated in *GBT0419/0419*.

Upon DOX stress, induction of *rxraa* and *rxrab* transcripts was detected in the cardiac tissues of wild-type fish at both the acute and chronic phases of AIC (fig. S4D). In *GBT0419/0419* fish, we noted that DOX induces hyperactivation of *hoxb5a* and *hoxb5b*, two RA-targeted

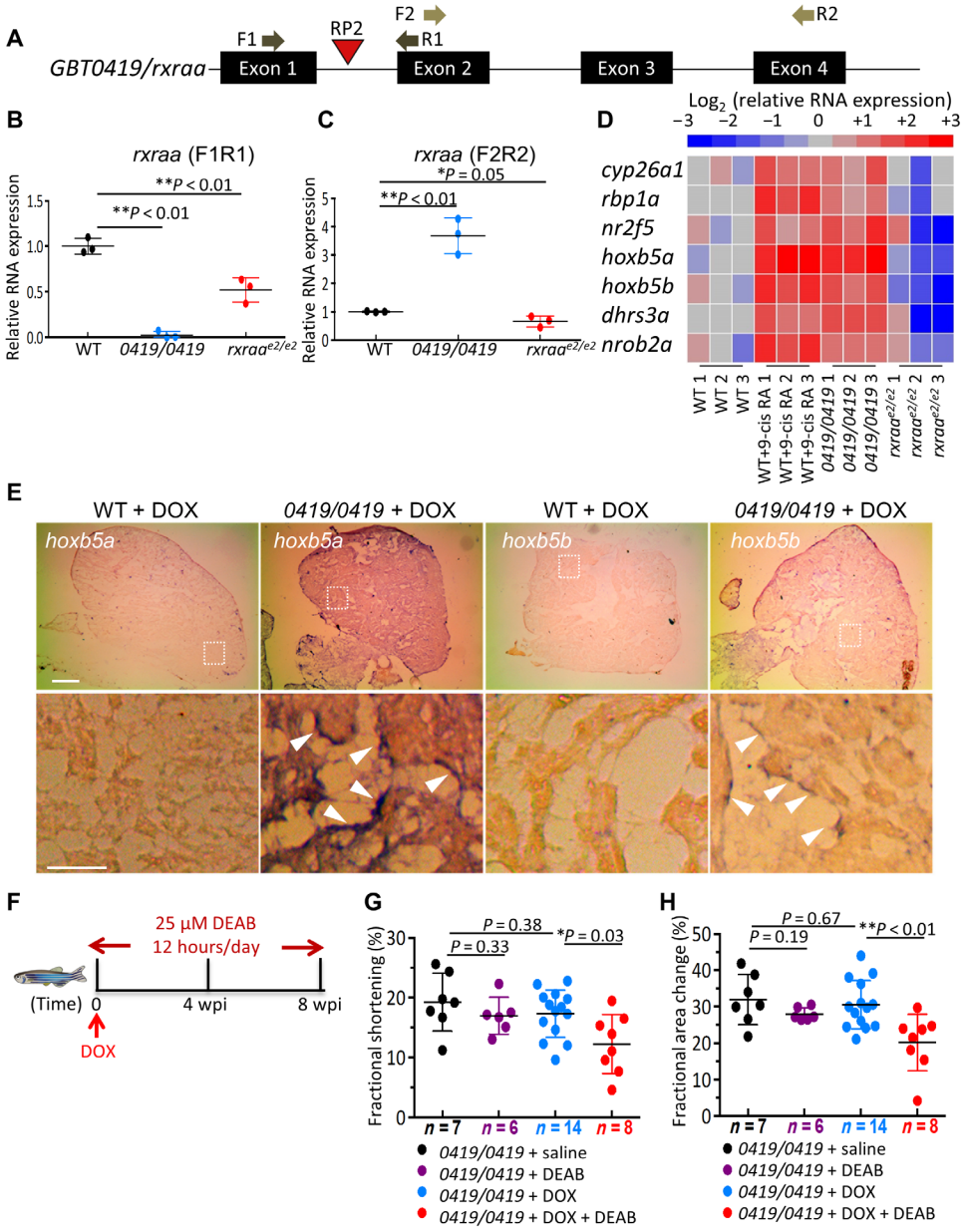

Fig. 3. Activation of RA signaling is responsible for the cardioprotective effects associated with *GBT0419*. (**A**) Schematics showing locations of *rxraa* primers for quantitative reverse transcription PCR. Primer pair 1 (F1R1) targets exon 1 and exon 2 flanking the RP2 insertion locus. Primer pair 2 (F2R2) targets exon 2 and exon 4, which amplify *rxraa* transcripts containing C-terminal exons. (**B**) Relative degree of exon 1–exon 2 splicing *rxraa*, as measured by primer pair 1, in *GBT0419/0419* and *rxraa*$^{e2/e2}$. (**C**) Relative expression of *rxraa* transcripts, as measured by primer pair 2, in *GBT0419/0419* and *rxraa*$^{e2/e2}$. (**D**) Heat map of the relative mRNA expression levels of genes regulated by RA signaling in *GBT0419/0419* and *rxraa*$^{e2/e2}$. Values are shown as the $\log_2$ transformation of relative mRNA expression normalized to the mean value of WT. *actb2* was used as an internal control. In (B) to (D), RNA was extracted from a pool of 20 fish embryos at 2 dpf, which was considered a single biological replicate (represented as a single dot). Samples were collected in triplicate. (**E**) *hoxb5a* and *hoxb5b* expression detected by in situ hybridization on adult hearts at 24 hours after DOX stress. The bottom panels show a higher-magnification view of the dotted box area in the top panels. Arrowheads indicate endocardial expression. $n = 3$ for each group. Scale bars, 100 μm (top panel) and 20 μm (bottom panel). (**F**) Schematic of the schedule for DEAB administration and DOX injection. (**G**) Ventricular fractional shortening of *GBT0419/0419* adult fish with or without DEAB treatment upon DOX stress at 8 wpi. (**H**) Ventricular fractional area change in *GBT0419/0419* adult fish with or without DEAB treatment upon DOX stress at 8 wpi. Each dot represents an individual ventricle. Error bars indicate SD. *$P < 0.05$ and **$P < 0.01$; one-way ANOVA followed by Tukey's post hoc test was used.

genes, specifically in endocardial cells at 24 hours after stress (Fig. 3E), further supporting *GBT0419* as a gain–of–RA function mutant. To test the hypothesis that such hyperactivated RA signaling confers, at least in part, the salutary effects of *GBT0419*, we inhibited RA signaling with diethylaminobenzaldehyde (DEAB) (Fig. 3F), a compound inhibitor of the aldehyde dehydrogenase 1 family, member A2 (Aldh1a2), which is the major enzyme for endogenous RA synthesis. Chronic treatment with DEAB (25 μM, 12 hours/day) reduced the activity of RA signaling (fig. S5A), exacerbated the mortality of *GBT0419/0419* during AIC (fig. S5B), and markedly attenuated its cardioprotective

effects, as evidenced by the reduced ventricular pump function at both 4 wpi (fig. S4, C to E) and 8 wpi (Fig. 3, G and H).

Endothelial-specific overexpression of *rxraa* is therapeutic for AIC

To directly test the hypothesis that gain of *rxraa* function in endothelial cells is therapeutic against AIC, we generated *Tg(βactin2:loxP-mCherry-stop-loxP-rxraa-EGFP)*, an inducible transgenic line that is hereafter termed *Tg(βact2:RSRxraa)* (Fig. 4A). The effectiveness of this binary expression system was indicated by the induced EGFP fluorescence (fig. S6A), the induced Rxraa-EGFP protein (fig. S6B), and the activated RA-targeted genes (fig. S6C) in *Tg(βact2:RSRxraa); Tg(HSP70:EGFP-Cre)* double-transgenic fish upon heat shock. Of note, this ectopic overexpression of Rxraa-EFGP protein did not affect the expression of endogenous *rxraa* and other RXR genes (fig. S6, D and E, and data not shown).

Tg(βact2:RSRxraa) was then bred into *Tg(kdrl:CreER)* or *Tg(cmlc2:CreER)* to overexpress *rxraa* in either endothelial cells or cardiomyocytes, respectively. The lineage-specific inductions of Rxraa-EGFP protein were noted from embryogenesis (Fig. 4, B and D) through adulthood (Fig. 4, C and E), and the identity of the chimeric protein in adult cardiac tissues was confirmed by Western blotting (Fig. 4F). Upon DOX stress, endothelial-specific overexpression of *rxraa* appeared to be therapeutic for AIC, as indicated by rescued ventricular function, restored exercise capacity, and improved survival (Fig. 4, G, I, and K). In contrast, cardiomyocyte-specific *rxraa* overexpression did not exert any salutary effects (Fig. 4, H and J).

We also assessed the effects of epicardial overexpression of *rxraa* by generating *Tg(tcf21:CreER);Tg(βact2:RSRxraa)* double-transgenic fish. While induction of the Rxraa-EGFP fusion protein was noted in embryonic *tcf21*$^+$ cells (6 dpf) at the junction between the outflow tract and the ventricle (fig. S6F), we did not note any sustained protective effects on AIC (fig. S6G). Of note, these data should be cautiously interpreted because a previous study (*27*) suggested that the *βactin2* promoter might not drive gene expression efficiently in the *tcf21*$^+$ epicardial cells. We also did not detect consistent induction in adult fish hearts at 3 months of age (fig. S6F).

RXRA agonists are therapeutic for AIC during the acute phase, but not during the chronic phase or as pretreatment, in adult zebrafish

Having identified endothelial RXRA as the precise therapeutic target for AIC, we went on to translate our findings by studying six commercially available RXRA-activating compounds [including all-trans RA (ATRA); table S2A]. We first tested these compounds in high-throughput zebrafish embryos at 1 to 3 dpf. To avoid teratogenic effects associated with RA signaling activation, we determined the median lethal dose (LD_{50}) of each compound (fig. S7A). While four compounds at 20 to 50% of the corresponding LD_{50} resulted in pericardial edema (fig. S7B), all six compounds appeared to be safe when administered at approximately 1% of LD_{50} (table S2A). We then adopted an embryonic zebrafish AIC model (*28*) to assess the therapeutic effects (fig. S7C). Similar to the rescued ventricular shortening fraction, the heart rate, and the survival rate in *GBT0419/0419* embryos (data not shown), we found that administration of isotretinoin, SR11237, and bexarotene at the doses of 1% LD_{50} exerted therapeutic benefits for both survival and cardiac functions (fig. S7, D to F).

To further develop *RXRA*-based therapy, we decided to test isotretinoin and bexarotene, two FDA-approved compounds, in an adult zebrafish AIC model. Both RXRA agonists were delivered via a daily oral gavage, and the doses (24 μg/day per fish for isotretinoin and 97 μg/day per fish for bexarotene) were derived from the FDA-recommended doses for human patients (table S2B). At these doses, a one-time gavage of either compound was able to activate *rxraa* expression in adult fish hearts within a 24-hour cycle (fig. S8A). Given that the adult fish AIC model progresses from the acute phase to the chronic phase at 4 wpi (*12*), we delivered compounds at three time windows, i.e., 1 week before DOX administration (pretreatment), 1 to 4 wpi (acute phase of AIC with normal EF), and 5 to 8 wpi (chronic phase of AIC with reduced EF) (Fig. 5, A, D, and G). Therapeutic effects were only noted when compounds were administered during the acute phase of AIC, as shown by increased survival (Fig. 5B) and improved ventricular pump function at 4 wpi (data not shown), which can last weeks after the cessation of treatments (at 8 wpi; Fig. 5C). In contrast, treatment at the chronic phase was ineffective, as indicated by the unimproved survival and ventricular function (Fig. 5, E and F), as was use of the compounds as pretreatment (Fig. 5H).

Activation of RXRA repairs damaged tight junctions via regulating ZO-1 in endothelial cells during AIC

To gain mechanistic insights into the cardioprotective effects of endothelial RXRA activation during AIC, we studied these two RXRA agonists using cultured human coronary artery endothelial cells (HCAECs). By checking several endothelial signaling pathways that have been previously related to AIC pathogenesis (fig. S8E) (*2*), we found that both *tight junction protein 1 (TJP1)* and *endothelial nitric oxide synthase (eNOS)* were transcriptionally activated in isotretinoin-treated DOX-stressed HCAECs (fig. S8F). We decided to focus on *TJP1*, which encodes a tight junction protein Zonula occludens–1 (ZO-1), for two reasons. First, while the tight junctions in cardiac endothelial cells form a membrane barrier to regulate paracellular permeability (*29*), a recent study suggested that circulating DOX can disrupt ZO-1 structure and increase its exposure to cardiomyocytes (*5*). Second, two independent studies showed that activation of RA signaling can stimulate the expression of ZO-1 and other tight junction proteins in columnar epithelial cells (*30*) and brain endothelial cells (*31*). Thus, we posited that the therapeutic effects of RXRA activation might be ascribed to the regulation of *TJP1*. We found that treatment with DOX at multiple doses markedly reduced the expression of ZO-1 without incurring apoptosis (fig. S8G), which can be attenuated if cotreated with either isotretinoin (100 nM) or bexarotene (10 nM) (Fig. 6A). In zebrafish, we also found that RXRA agonists activate *tight junction protein 1a (tjp1a)* or *tight junction protein 1b (tjp1b)*, two zebrafish orthologs of *TJP1*, in AIC zebrafish endothelial cells (Fig. 6C) that were labeled by the *Tg(fli1a:EGFP)* transgene and isolated by fluorescence-activated cell sorting (Fig. 6B).

To test the hypothesis that the therapeutic effects of RXRA activation on AIC are ascribed to regulation of the endothelial barrier, we assessed tight junction formation. In the adult zebrafish AIC model, we noted a disrupted endothelial Zo-1 pattern at 5 days postinjection, which could be rescued by daily gavage with either isotretinoin or bexarotene (Fig. 6D). This observation was conserved in cultured HCAECs, as DOX treatment disrupted the native peripheral membrane structure of ZO-1, which could be prevented by cotreatment with either RXRA agonist (Fig. 6E). Last, to directly test the endothelial barrier hypothesis, we performed a cell permeability assay on the monolayer

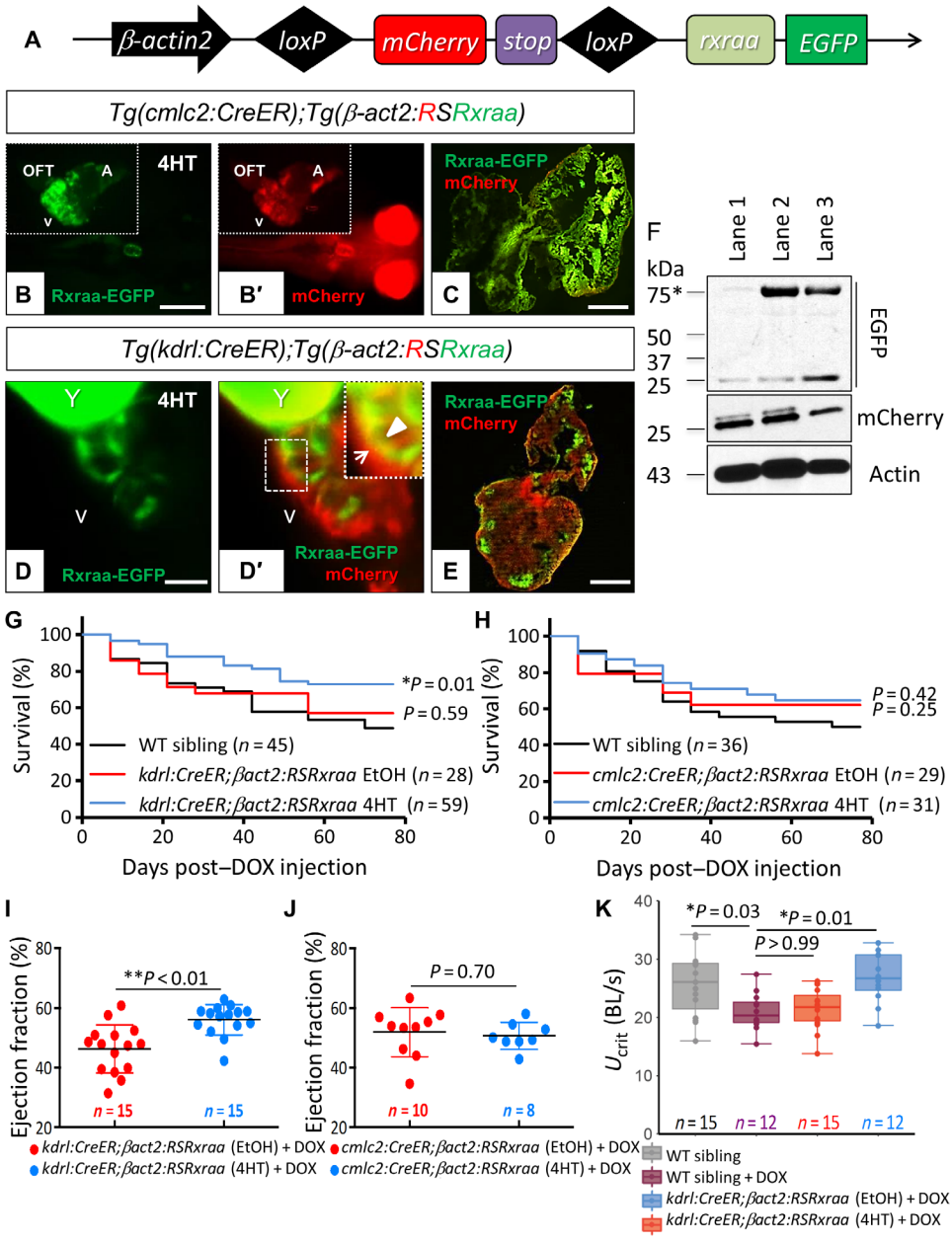

Fig. 4. Endothelial-specific overexpression of *rxraa* protects against AIC in vivo. (**A**) Schematic of the *rxraa* conditional transgenic line. (**B**) The green channel shows cardiomyocyte-specific *rxraa* overexpression at 6 dpf. A, atrium; V, ventricle; OFT, outflow tract. (**B'**) The red channel of the same view as (B) shows the original mCherry expression. Insets show the same heart after dissection. (**C**) Heart from a 3-month-old fish showing cardiomyocyte-specific *rxraa* overexpression. Scale bar, 500 μm. (**D**) The green channel shows endothelial-specific *rxraa* overexpression at 6 dpf. Y, yolk with autofluorescence. (**D'**) The merged channel with the same view as (D) shows mCherry and Rxraa-EGFP expression. The inset shows a higher-magnification view of the dotted area. The triangle indicates the endothelial layer; the arrowhead indicates the nonendothelial layer. Scale bar, 100 μm. (**E**) Heart from a 3-month-old fish showing endothelial-specific *rxraa* overexpression. Scale bar, 500 μm. (**F**) Western blot of adult ventricles. The predicted size of the induced Rxraa-EGFP fusion protein is 75 kDa (indicated by an asterisk). Actin was used as an internal control. Lane 1, *Tg(βact2:RSRxraa)*; lane 2, *Tg(βact2:RSRxraa);Tg(kdrl:CreER)* + 4HT; lane 3, *Tg(βact2:RSRxraa);Tg(cmlc2:CreER)* + 4HT. (**G** and **H**) Kaplan-Meier survival curves showing the survival of DOX-stressed adult fish with endothelial-specific (G) or cardiomyocyte-specific (H) *rxraa* overexpression. (**I** and **J**) Ventricular EF of adult hearts with endothelial-specific (I) or cardiomyocyte-specific (J) *rxraa* overexpression at 8 wpi. (**K**) Swimming capacity of fish, with or without endothelial-specific *rxraa* overexpression. Error bars indicate SD. *P < 0.05 and **P < 0.01; log-rank test in (G) and (H); unpaired Student's t test in (I) and (J); Kruskal-Wallis test followed by Tukey's post hoc test in (K).

of cultured HCAECs with fluorescein isothiocyanate (FITC) and found that cotreatment with both isotretinoin and bexarotene diminished the increased cell permeability resulting from DOX exposure (Fig. 6F).

DISCUSSION

The present work is based on a suppressor screen–like platform in adult zebrafish that can be used to systematically find new gene modifiers for AIC. Here, we demonstrated that the highly efficient

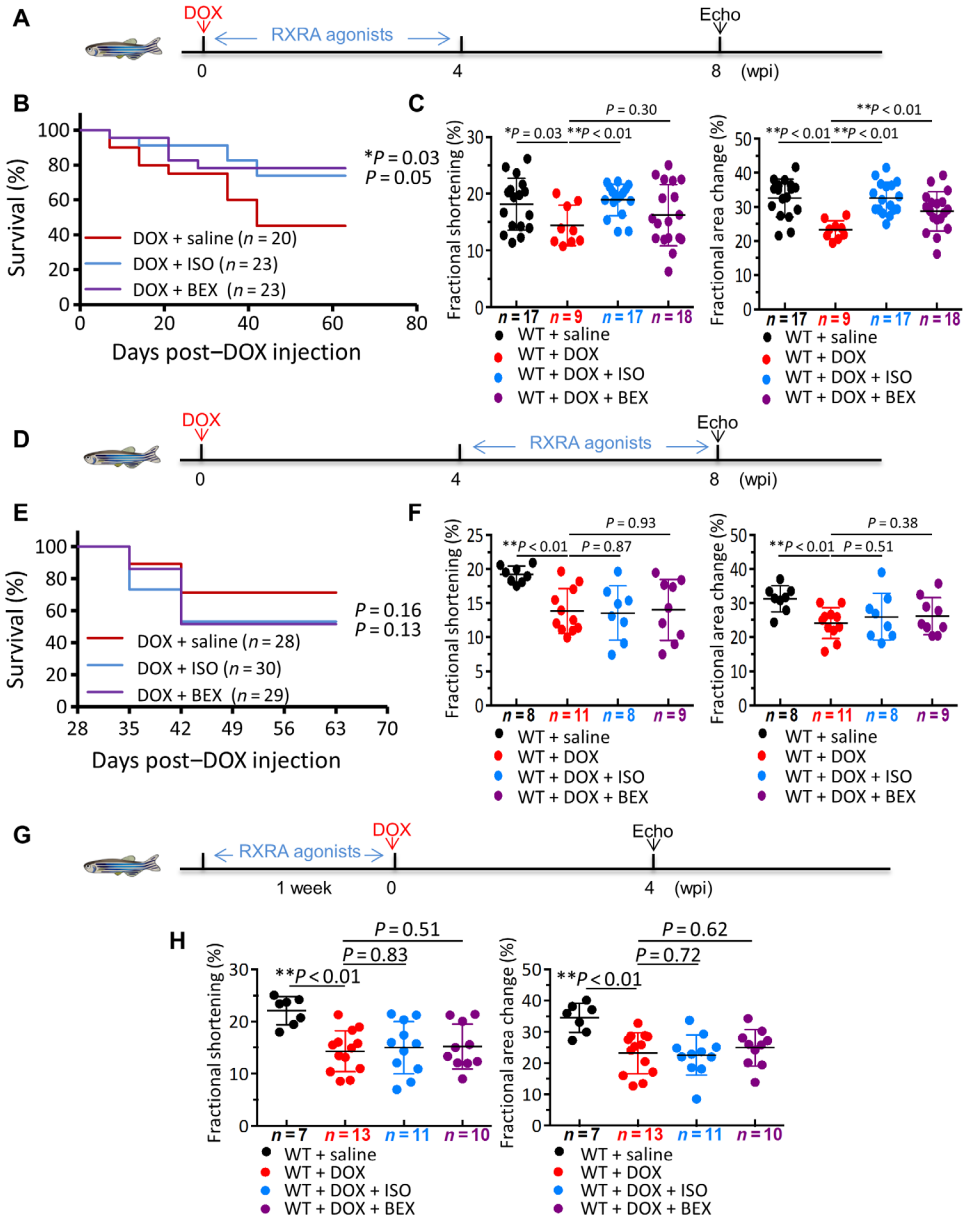

Fig. 5. RXRA agonists exert stage-dependent cardioprotective effects on AIC. (**A**, **D**, and **G**) Schematics of the schedules for RXRA agonist treatment at the early (1 to 4 wpi) or late (4 to 8 wpi) phase or as pretreatment (1 week before DOX) in the adult fish AIC model. A single bolus of DOX was injected as indicated in red. RXRA agonists were delivered daily by oral gavage. Isotretinoin (ISO) and bexarotene (BEX) were administered at clinically relevant doses, as listed in table S2B. High-frequency echocardiography was performed at the indicated time points to quantify cardiac functions. Saline was used as a control. (**B** and **C**) Indices of treatment with RXRA agonists during the early phase. (**E** and **F**) Indices of treatment with RXRA agonists during the late phase. (**H**) Indices of treatment with RXRA agonists during the pretreatment phase. (B and E) Kaplan-Meier survival curves show the survival of adult fish after DOX stress. (C, F, and H) Fractional shortening and fractional area change of adult ventricles at the respective time of echo after DOX stress. Error bars represent SDs. *$P < 0.05$ and **$P < 0.01$; log-rank test was used in (B) and (E) for comparisons with the saline group; one-way ANOVA followed by Tukey's post hoc test was used in (C), (F), and (H).

zebrafish model enables unbiased genetic studies to rapidly uncover mechanisms of new AIC genes at the lineage resolution, allowing the generation of knowledge to guide future translational efforts. Specifically, through comprehensive genetic and pharmacological studies of the first salutary modifier that emerged from our pilot screen, we made the following novel discoveries prompting an *RXRA*-based therapy. First, we provided multiple lines of genetic evidence indicating *RXRA* as a feasible therapeutic target for AIC. Second, we uncovered a spatially predominant nature of *RXRA*-based therapy in endothelial cells and further elucidated that one of the underlying mechanisms is the repair of DOX-induced damage to the endothelial barrier. Third, we uncovered the temporally predominant nature of the *RXRA*-based strategy, which shall be exerted during the early phase of AIC.

Before our genetic studies, the cardioprotective potential of RA signaling activation has been recognized from a pharmacological perspective (*32*). Treatment with ATRA, in particular, has been shown to benefit the cardiovascular system under multiple pathological

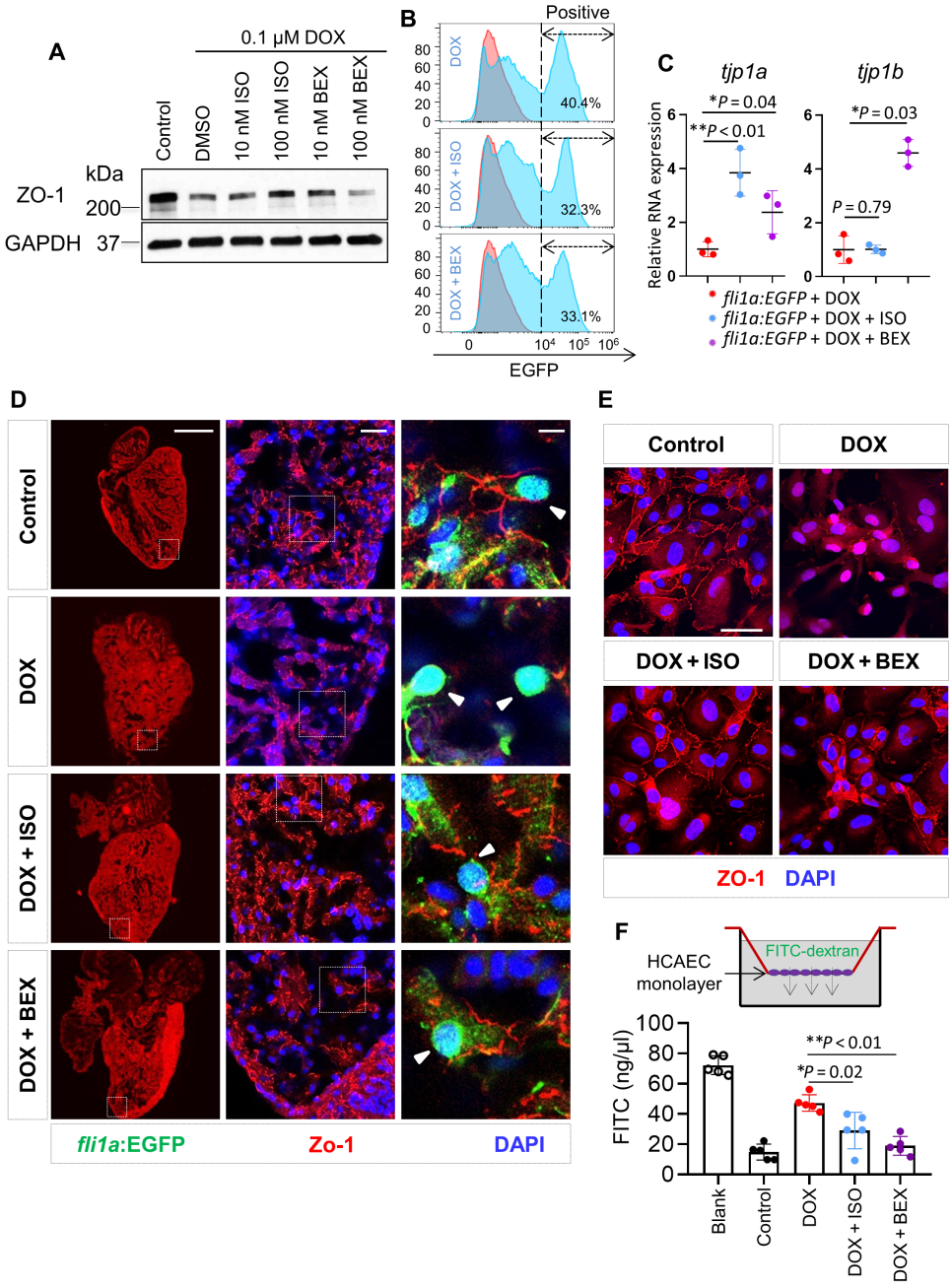

Fig. 6. Treatment of RXRA agonists reduces endothelial cell permeability by regulating ZO-1 functions during the early stage of AIC. (**A**) Western blot of ZO-1 expression in cultured HCAECs. Glyceraldehyde 3-phosphate dehydrogenase (GAPDH) was used as an internal control. The control group received no treatment. (**B**) Separation of the endothelial cell population from *Tg(fli1a:EGFP)* adult zebrafish ventricular tissues. A fluorescence-activated cell sorting was conducted at 24 hours post–DOX injection with or without oral gavage of RXRA agonists. The red area shows the cell distribution of the WT control (no fluorescence). (**C**) Real-time quantitative PCR shows *tjp1a* and *tjp1b* mRNA expression in separated adult zebrafish endothelial cells. *actb2* was used as an internal control. (**D**) Representative Zo-1 structure in endothelial cells in *Tg(fli1a:EGFP)* adult zebrafish heart at 5 days postinjection. The middle panels show higher magnification of the boxed area on the left; the far right panels show higher magnification of the boxed area in the middle. Arrowhead indicates endothelial cells. DOX and RXRA agonists were delivered via intraperitoneal injection or oral gavage, respectively. The control group was injected with saline and gavaged with dimethyl sulfoxide (DMSO). $n > 3$ for each group. Scale bars, 500, 40, and 5 μm, from left to right. (**E**) Immunostaining shows the ZO-1 structure in HCAECs upon DOX stress and treatment with RXRA agonists. DOX (0.1 μM), 100 nM ISO, and 10 nM BEX were used. The control was treated with DMSO. $n = 3$ for each group. Scale bar, 20 μm. (**F**) Top: A schematic showing the design of the HCAEC permeability assay. Lower FITC concentrations were detected in the outer well after FITC (1 μg/μl) was added to the inner well for 30 min of incubation. The blank group had no HCAECs, and the control was treated with DMSO. DOX (0.1 μM), 100 nM ISO, and 10 nM BEX were used. $^*P < 0.05$ and $^{**}P < 0.01$; one-way ANOVA followed by Tukey's post hoc test was used in (C) and (F).

conditions. Given that ATRA primarily binds to retinoic acid receptors (RARs), the cardioprotective effects of RA activation have been generally attributed to RARs. Nevertheless, recent studies also prompted the therapeutic effects of pan-RXR agonists (*33*), although treatments with RXR and RAR agonists were associated with slightly different physiological alterations in vivo (*23*). Here, we provide genetic and pharmacological evidence revealing *RXRA* as an AIC gene with therapeutic capacity. Our data consisted of a human GWAS analysis; experiments using a panel of zebrafish lines including *GBT0419*, an *rxraa* TALEN mutant, and *rxraa* gain-of-function transgenic lines; and pharmacological studies of RXRA agonists and an RA inhibitor (DEAB). Together with the recent discovery of *RARG* as an AIC susceptibility gene (*9*) and the observation of aberrant expression of *RARA* in a human-induced pluripotent stem cell–derived cardiomyocyte AIC model (*34*), our data underscore RA as a vital signaling pathway in AIC pathogenesis. The establishment of *RXRA* as a therapeutic target prompted future studies to examine whether *RARA* or *RARG* can be manipulated to exert therapeutic effects. Because *RARG* has been reported to regulate the expression of *TOP2B* (*9*), the pertinence of this myocardium-based mechanism with endothelial *RXRA* during AIC pathogenesis warrants further investigation.

Historically, mechanistic studies of candidate cardioprotective pathways have been disproportionally emphasized in cardiomyocytes. The contribution of noncardiomyocytes in AIC has only begun to be appreciated recently (*35*). Partially inspired by early genetic studies (*17*–*19*) that defined noncardiomyocyte requirements of *RXRA* during mammalian cardiac morphogenesis, we systematically assessed the functions of *rxraa* in endothelial cells, cardiomyocytes, and epicardial cells. Both lineage-specific rescue and transgenic experiments indicated that the observed *rxraa*-based cardioprotection was mainly ascribed to genetic manipulation in endothelial cells, not cardiomyocytes. Our data demonstrated that endothelial gain of *rxraa* function alone in AIC adult zebrafish is sufficient for long-term physiological benefits, including improved survival, cardiac function, and exercise capacity. Collectively, our data suggest that future studies of RA-related genes in AIC and potentially other cardiovascular diseases need to consider the contribution of endothelial cells, in addition to direct functions within cardiomyocytes.

Within cardiac endothelial cells, we uncovered that *RXRA* activation functions in repairing the damaged tight junction barrier, which could theoretically prevent exposure of cardiomyocytes to circulating DOX and the subsequent development of decompensated cardiomyopathies. Notably, RXRA activation could have other potential benefits in the endothelium. For example, activation of RA signaling has been shown to promote functions of vascular endothelium via boosting eNOS activity and nitric oxide production (*36*). We detected transcriptional activation of *eNOS* in isotretinoin-treated HCAECs (fig. S8, E and F). Moreover, activation of RA signaling could promote proliferation of endothelial cells, as has been shown in vasculogenesis, development of the yolk sac (*37*, *38*), and heart regeneration (*39*). Future studies are warranted to test these additional potential mechanisms and to examine how endothelial *RXRA* signaling interacts with other AIC-protective targets such as *vascular endothelial growth factor-B* (*VEGF-B*) (*35*). This line of studies will significantly advance our understanding of the contribution of cardiac endothelium to AIC, a currently understudied area.

Our present genetic framework provides useful spatially and temporally predominant information that might guide further translation of *RXRA*-based therapies. When gene-based therapies are pursued, an endothelial-specific promoter could be integrated into molecular designs; when compound-based therapies are pursued, technologies that facilitate endothelium-preferred drug delivery (*40*) shall be considered. Consistent with the observation that clinical endothelium dysfunctions were typically observed during the early stage of AIC (*41*), we found that treatment with RXRA agonists exerts the best therapeutic benefits when administered during the acute AIC phase in adult zebrafish. Given that the administration of dexrazoxane is also recommended during early AIC (*42*), further studies should be conducted to compare these two therapies and to explore the possibility of cotreatment for synergistic cardioprotective effects. We highly anticipate the acceptance of RXRA-based clinical trials involving patients with cancer because RXRA agonists are also being actively developed as anticancer agents (*43*), and combinational therapies with DOX have already been explored in one recent trial (*44*). It is less likely that RXRA agonists will compromise the antineoplastic effects of anthracyclines.

We acknowledge limitations associated with our compound-based studies (Fig. 5) as none of these compounds are RXRA-specific agonists, despite the fact that they were selected because of their capability to trigger the activation of *rxraa* in the zebrafish heart (fig. S8A and data not shown). Besides activating RXRA, these agonists may stimulate expressions of other RXR or RAR genes (fig. S8B). Given that RXRA is a pleotropic receptor that can form homodimers, heterodimers with RARs, and permissive heterodimers such as PPAR/RXR and LXR/RXR (*16*), future studies are needed to discern precisely which receptor complex confers the therapeutic effects of these compounds. Our preliminary data suggested that isotretinoin and bexarotene do activate expression of *raraa* and the target genes for LXR/RXR, but not PPAR/RXR (fig. S8, B to D). We did not genetically test whether *rxraa* is exclusively required for the therapeutic effects of these agonists, because zebrafish *rxrab* may compensate for certain functional loss of *rxraa*. Moreover, because our screen of the RXRA agonists was carried on an embryonic AIC model at a single dose of 1% LD_{50}, which might not be optimal for every tested compound, our data cannot be interpreted as excluding the cardioprotective effects of RXRA agonists with lower priority in this study such as ATRA and 9-cis RA.

Cautions also must be taken considering the limitations associated with adult zebrafish as an animal model. For example, unlike mouse genetics, transgenic fish with cardiomyocyte-specific overexpression of *rxraa* did not show any noticeable cardiac phenotypes up to 1 year old. One potential explanation could be that the strong regenerative capacity of the zebrafish cardiomyocytes rendered them more resilient to biomechanical stresses. To test the conservation, here, we acquired some evidence from the GWAS analysis of *RXRA* in patients with AIC and the conserved tight junction–related mechanism in cultured HCAECs. Further validation in rodents and/or large mammals is needed before testing *RXRA*-based therapies, such as repurposing FDA-approved RXRA agonists, for clinical uses.

In summary, our data demonstrate adult zebrafish as an efficient in vivo model for deciphering underlying mechanisms for a new AIC gene. Our approach can be simply extended to any AIC genes that emerge from either the zebrafish forward genetic screen or human genetic studies. Inferred from our pilot screening, it is estimated that ~200 zebrafish genetic modifiers for AIC exist across the genome (*13*). Like *GBT0419*, some of these modifying mutants might exert salutary effects and shall be pursued as new candidate therapeutic targets. Priority shall be given to genes, such as *RXRA*, with supporting

human genetic data. We also anticipate that the zebrafish-based forward genetic screening efforts can be extrapolated to other types of cardiomyopathies, which shall substantially facilitate the development of gene- and mechanism-based therapeutic strategies.

MATERIALS AND METHODS

Zebrafish husbandry

Adult zebrafish were maintained under a light-dark cycle (14 hours of light and 10 hours of darkness) at 28.5°C. Zebrafish embryos were maintained in a 10-mm petri dish with E3 water at 28.5°C up to 7 dpf. All animal experiments were approved by the Mayo Clinic College of Medicine Institutional Animal Care and Use Committee (protocol A00002783-17).

Generation of the *rxraa*$^{e2/e2}$ mutant

TALENs targeting exon 2 of *rxraa* were designed with ZiFiT (http://zifit.partners.org/ZiFiT/ChoiceMenu.aspx). The N-terminal TALEN-binding sequence was 5′-tcagagaggacgagcaga-3′, and the C-terminal TALEN-binding sequence was 5′-cggaatgtgtgctcttca-3′. Both TALENs were constructed by using the Golden Gate kit. Capped mRNAs were synthesized by using the mMESSAGE mMachine T3 kit (Ambion). TALEN mRNAs (15 pg to 1 ng) were injected into wild-type embryos at the one-cell stage. Founder fish with desired genomic lesion were identified by genotyping (forward primer, 5′-tccatagggttcctgaagc-3′; reverse primer, 5′-tctgaatatgcacgttacctg-3′). The amplified PCR products were digested with restriction enzyme HypCH4IV. The precise genomic lesion was then determined by Sanger sequencing. After the mutants were generated and sequenced, the founders were outcrossed to WIK fish for >5 generations to eliminate any potential background mutations.

Generation of the *Tg*(β*actin2:loxP-mCherry-stop-loxP-rxraa-EGFP*) transgenic line

The transgenic line was generated using the Tol2/Gateway system. The *loxP-mCherry-stop-loxP* fragment was amplified from the Hot-Cre plasmid (Addgene plasmid no. 24334) and inserted into Kpn I/Eco RI sites of the pENTRI1a vector from the Tol2Kit. Full-length *rxraa* complementary DNA (cDNA) (ENSDART00000141380.3) was amplified from adult fish heart cDNA pool using forward primer 5′-atagcggccgcatggaaaccaaacctttctt-3′ and reverse primer 5′-gcggatatcttgtcatttggtgtggagcttct-3′. A clone with the correct sequence of the full-length *rxraa* was confirmed by Sanger sequencing, and the gene was then cloned into the pENTRI1-*loxP-mCherry-stop-loxP* vector. To generate the final construct, p5E-*bactin2*, pENTRI-*loxP-mCherry-stop-loxP-rxraa*, p3E-*EGFP-polyA*, and pDestTol2pA were combined together with the Gateway LR clonase II plus enzyme (Thermo Fisher Scientific). The final construct was confirmed by gel electrophoresis. Fifty to 100 ng of the final construct, together with 100 ng of transposase mRNA, was then injected into WIK embryos at the one-cell stage. Founder fish (F0) were identified on the basis of mCherry fluorescence. Transgenic fish used for experiments were from F2 and F3 generations.

Conditional expressional system

Tg(HSP70:EGFP-Cre), *Tg(kdrl:CreER)*^{fb13}, *Tg(cmlc2:CreER)*^{pd10}, and *Tg(tcf21:CreER)*^{pd42} were used in the current study. To activate the heat shock promoter, double-transgenic fish were incubated at 37°C for 1 hour at 1 dpf. The EGFP reporter integrated in *Tg(HSP70:EGFP-Cre)* can transiently emit fluorescence about 2 to 6 hours after incubation, and the signal dissipates within the next 48 hours. To activate a tissue-specific promoter, embryos from double-transgenic fish were incubated in 10 μM 4HT (Sigma-Aldrich) from 0 to 6 dpf for *Cre-loxP* recombination. E3 water containing 4HT was refreshed every 24 hours. For subsequent experiments on the adult stage, embryos with effective recombination were selected on the basis of eye and body fluorescence (assessed using a Zeiss microscope) by 6 dpf. Only recombinant-positive embryos were raised and used in the subsequent experiments.

Compound treatment in zebrafish

For DEAB treatment, compounds were dissolved in dimethyl sulfoxide (DMSO) to create a stock solution. Adult zebrafish were incubated overnight (about 12 hours) in 500 ml of system water containing DEAB in a 1-liter mini tank. We tested DEAB at various concentrations (250, 100, 50, 25, and 2.5 μM) and determined that the maximum concentration that did not result in fish death after an overnight incubation was 25 μM. Adult fish were incubated in 25 μM DEAB for 12 hours per day for 2 months. Fresh DEAB water was used daily, and the density of fish was maintained at <5 fish/500 ml.

For treatment of RXRA agonists at embryonic stages, embryos were incubated in E3 water containing compounds at the desired concentrations. 1-Phenyl-2-thiourea (PTU) was used to remove pigmentation. For administration of RXRA agonists to adult fish, bexarotene and isotretinoin were delivered via oral gavage at the desired dose (table S2B) on a daily basis.

Adult and embryonic AIC model

For adult zebrafish, DOX was delivered via intraperitoneal injection (20 mg/kg), as previously described (*12*). For embryonic fish, DOX was delivered from 24 to 72 hpf; DOX was dissolved in E3 water containing 100 μM PTU, and the solution was refreshed every 24 hours.

Quantification of ventricular pump function via an ex vivo system

We used our recently developed Langendorff-like perfused zebrafish heart technique (*25*). Briefly, hearts were isolated from tricaine-anesthetized fish, cannulated by using 34-gauge ultrathin catheters through the atrioventricular canal visualized with a stereomicroscope Leica M165C (Leica, Germany), paced with an isolated stimulator MyoPacer (IonOptix; ~15 V, 10 ms, 2 Hz), and perfused using a peristaltic pump EP-1 Econo Pump (Bio-Rad). Images were acquired by using a complementary metal-oxide semiconductor camera (MU1403; AmScope; 66 frames/s). All experiments were conducted at room temperature.

End-diastolic volume (EDV) and end-systolic volume (ESV) were calculated with the area-length formula

$$V = 2/3\, A_{AL} \times L_{AL}$$

where A_{AL} is the area of the base of the ventricle in transverse projection and L_{AL} is the long length of the ventricle in longitudinal projection. To get two perpendicular projections of the ventricle images, we used a 45° angle aluminum mirror (Thorlabs). The images were analyzed using the ImageJ software [National Institutes of Health (NIH)]; three cardiac cycles were analyzed to obtain averaged EDV and ESV values. EF was calculated as follows

$$EF = 1 - ESV/EDV$$

Quantification of heart pump function via a high-frequency echo system

High-frequency echocardiography was leveraged when quantification of pump function needed to be conducted at multiple time points on the same adult zebrafish heart (Figs. 3 and 5). All ultrasound movies were documented with a Vevo 3100 high-frequency imaging system (FUJIFILM VisualSonics Inc., Toronto, Canada) equipped with a 50-MHz linear array transducer (MX700). Acoustic gel (Aquasonic 100, Parker Laboratories Inc.) was applied over the surface of the transducer to provide adequate coupling with the tissue interface. Zebrafish were anesthetized with tricaine (0.16 mg/ml), placed ventral side up, and held in place with a soft-sponge stage. The MX700 transducer was positioned above the zebrafish to provide a sagittal imaging plane of the heart. B-mode images were acquired with an imaging field of view of 9.00 mm in the axial direction and 5.73 mm in the lateral direction, a frame rate of 123 Hz, with medium persistence and a transmit focus at the center of the heart. Images were quantified with the Vevo LAB workstation. Data were acquired and processed as previously described (*45*). Ventricular chamber dimensions were measured from B-mode images using the following two indices: fractional shortening = (EDD − ESD)/EDD; fractional area change = (EDA − ESA)/EDA. EDD and ESD were the perpendicular distances from the ventricular apex to the ventricular basal line at the end-diastolic and end-systolic stages, respectively; EDA and ESA were defined as the areas of the ventricular chamber at the end-diastolic and end-systolic stages, respectively. For each index, measurements were obtained during three to five independent cardiac cycles per fish to determine average values.

Swimming tunnel assay

A swimming challenge was conducted on adult zebrafish using a swim tunnel respirometer (Mini Swim 170, Loligo Systems, Tjele, Denmark), with a protocol that was previously reported. U_{crit} was defined as the maximum water speed that fish were able to swim against while maintaining their position. Fish were fasted for 24 hours for synchronization before the test. Five to 10 fish were loaded into the swim tunnel and acclimated in a lower speed of 9 cm/s (200 rpm) of flowing water for 20 min. Water speed was then increased in steps of 8.66 cm/s (100 rpm) (U_{ii}) at 150-s intervals (T_{ii}) until all fish were exhausted and failed to resume swimming from a downstream screen. The highest water speed (U_i) against which fish were able to complete the 150-s swim test and the swimming duration time (T_i) in the next 150-s period were recorded for each fish. U_{crit} was calculated with the following formula

$$U_{crit} = U_i + U_{ii} \times (T_i/T_{ii})$$

and normalized to fish body length for intergroup comparisons.

Preparation of single-cell suspension from adult tissues and fluorescence-activated cell sorting

Five to 10 adult fish ventricles were dissected and cut into pieces with surgical scissors. Tissues were then transferred into a 1.5-ml tube containing 1 ml of HBSS buffer with collagenase/dispase (5 mg/ml; Roche) and collagenase 2 (5 mg/ml; Worthington) and put on a shaker at room temperature for 60 to 75 min. Samples were gently mixed by pipetting every 15 min. Ice-cold HBSS with 10% fetal bovine serum was used to wash the samples twice, and ACK buffer [0.15 M NH_4Cl, 1 mM $KHCO_3$, and 0.1 mM Na_2EDTA (pH 7.2)] was used to remove blood cells. All samples went through a 70-μm sterile cell strainer. Propidium iodide (1 μg/ml) was used to stain for dead cells. After PI staining, cells were acquired through an 11-color Attune NxT system (Life Technologies). Data were then analyzed by FlowJo software (Tree Star).

HCAEC culture

Primary HCAECs were purchased from the American Type Culture Collection (PCS-100-020) and cultured in vascular cell base medium (PCS-100-030) containing an endothelial cell growth kit (PCS-100-041) at 37°C. HCAECs at the fourth or fifth passage were used for DOX treatment. Culture medium containing DOX and isotretinoin or bexarotene was added together. All cells were harvested at 12 or 24 hours after DOX treatment.

For permeability assay, HCAECs were seeded at 1.5-fold of the confluent concentration on a ThinCert 0.4-μm translucent insert (Greiner) placed on a 24-well plate and grew for 48 hours. Cells were treated with DOX and RXRA agonists for another 24 hours. Medium in both the insert and outer wells were refreshed, and FITC (1 μg/μl) (4 kDa; Sigma-Aldrich) was added to the insert for 30-min incubation. Two hundred microliters of medium from the outer well was then used to quantify the FITC concentration using a microplate reader (Bio-Rad) at 490 nm.

Real-time quantitative PCR

For fish embryo studies, 20 embryos were pooled for RNA extraction. For adult fish studies, three freshly dissected tissues were pooled for RNA extraction. For primary cell culture, cells in a 60-mm plate were harvested as a single biological replicate. RNA was extracted using TRIzol (Bio-Rad) following the manufacturer's instructions. cDNA was synthesized by using Superscript III First-Strand Synthesis System (Invitrogen) and 100 to 500 ng of RNA. Real-time reverse transcription PCR assays were performed in 96-well optical plates (Thermo Fisher Scientific) using an Applied Biosystems VAii 7 System (Thermo Fisher Scientific). Levels of gene expression were normalized to either *glyceraldehyde 3-phosphate dehydrogenase* (*gapdh*) or *actin beta 2* (*actb2*). The data presented with heat map were generated using heatmap.2 function implanted in gplots package with R statistical software. Sequences for all PCR primers used in this study are available upon request.

Western blotting

Zebrafish embryos at 5 dpf or freshly dissected adult ventricular tissues were collected in 1.5-ml safe-lock tubes (Eppendorf) and mechanically homogenized (Blender tissue homogenizer; Next Advance Inc.) in radioimmunoprecipitation assay lysis buffer (Sigma-Aldrich) containing proteinase inhibitor, 1 mM phenylmethylsulfonyl fluoride, and stainless steel beads. Standard protocols of Western blotting were followed. For each sample, >20 μg of total protein was loaded on an SDS polyacrylamide gel. The following primary antibodies were used: anti-EGFP (1:2000) (Santa Cruz Biotechnology), anti-mCherry (1:1000; Novus Biologicals), anti–ZO-1 (1:1000; Invitrogen), and anti-cleaved caspase-3 (1:1000; Cell Signaling Technology). Anti-actin (1:2000) (Sigma-Aldrich) and anti-GAPDH (1:2000; Santa Cruz Biotechnology) were used as an internal control.

Immunofluorescence

Embryonic hearts were dissected by following a published protocol. Dissected embryonic hearts were fixed in 4% paraformaldehyde

before imaging. Adult cardiac tissues were freshly dissected and placed in molds with frozen section medium on dry ice. Frozen samples were transferred to −80°C overnight and subsequently sliced into 10-μm sections with a cryostat (Leica CM3050S). For endogenous mRFP, EGFP, and mCherry, images were obtained within 24 hours after dissection of embryonic and adult hearts. For immunostaining, sections of adult cardiac tissues were fixed in 4% paraformaldehyde and then subject to a standard protocol. Primary antibodies against Mef2 (1:200; Santa Cruz Biotechnology) and actinin (1:100; Sigma-Aldrich) were used. Quantification of the disarray of sarcomeres in Fig. 2H was conducted with ImageJ software (NIH). Intact Z-disc structures were counted from six randomly selected myofilaments for sections of each heart and were normalized by distance. To quantify apoptotic cells, TUNEL (terminal deoxynucleotidyl transferase–mediated deoxyuridine triphosphate nick end labeling) staining was conducted using an In Situ Cell Death Detection kit (Roche) following the manufacturer's instructions. All images were captured using a Zeiss Axioplan II microscope equipped with ApoTome.2 or a Zeiss confocal microsope, installed with ZEN software (Carl Zeiss).

Statistics

No sample sizes were calculated before performing the experiments, and no animals were excluded for analyses. Wild-type sibling zebrafish were used as a control for mutants or transgenic lines whenever possible. For homozygote mutant lines, age-matched wild-type zebrafish were used as controls. For survival analysis, experiments on >3 independent groups of fish were conducted. Log-rank tests were used to compare combined data from all experimental replicates. For dot plot graphs, values are displayed as means ± SD or means ± SEM. Unpaired two-tailed Student's *t* test was used to compare two groups; one-way analysis of variance (ANOVA) (or Kruskal-Wallis) test, followed by Tukey's post hoc test, was used for comparing three and more groups, and normality of the data was confirmed (or confirmed to be not). *P* values less than 0.05 were considered statistically significant. All statistical analyses were conducted with JMP 10 (SAS Institute Inc.) and Prism 6 (GraphPad) software.

SUPPLEMENTARY MATERIALS

Supplementary material for this article is available at http://advances.sciencemag.org/cgi/content/full/6/5/eaay2939/DC1

Fig. S1. RXRA is conserved across species and Rxraa expression in zebrafish.
Fig. S2. Endogenous *rxraa* expression in endothelial and myocardial cells of zebrafish hearts.
Fig. S3. Myocardial and epicardial RP2 reversions in *GBT0419/0419* have minimal cardioprotective effects against AIC.
Fig. S4. The generation of an *rxraa* zebrafish mutant by TALEN and the cardiac function indices for wild-type and *rxraa* mutants under AIC.
Fig. S5. Inhibition of RA signaling reduced survival and cardiac function in *GBT0419/0419* fish upon DOX stress.
Fig. S6. Ectopic expression of *rxraa* globally and in epicardial cells.
Fig. S7. Characterization of RXRA agonists on zebrafish embryos.
Fig. S8. Studies of isotretinoin and bexarotene on adult zebrafish and HCAECs.
Table S1. *RXRA* single-nucleotide polymorphisms in patients with AIC.
Table S2. Dosages of RXRA agonists used on zebrafish.
Movie S1. Cardiac functions of isolated hearts measured by a Langendorff-like system.
Movie S2. Cardiac functions of embryonic hearts.
Movie S3. Cardiac functions of adult hearts measured by echocardiography.

View/request a protocol for this paper from *Bio-protocol*.

REFERENCES AND NOTES

1. J. V. McGowan, R. Chung, A. Maulik, I. Piotrowska, J. M. Walker, D. M. Yellon, Anthracycline chemotherapy and cardiotoxicity. *Cardiovasc. Drugs Ther.* **31**, 63–75 (2017).
2. G. Minotti, P. Menna, E. Salvatorelli, G. Cairo, L. Gianni, Anthracyclines: Molecular advances and pharmacologic developments in antitumor activity and cardiotoxicity. *Pharmacol. Rev.* **56**, 185–229 (2004).
3. S. Zhang, X. Liu, T. Bawa-Khalfe, L.-S. Lu, Y. L. Lyu, L. F. Liu, E. T. H. Yeh, Identification of the molecular basis of doxorubicin-induced cardiotoxicity. *Nat. Med.* **18**, 1639–1642 (2012).
4. K. Chatterjee, J. Zhang, N. Honbo, J. S. Karliner, Doxorubicin cardiomyopathy. *Cardiology* **115**, 155–162 (2010).
5. E. L. Wilkinson, J. E. Sidaway, M. J. Cross, Cardiotoxic drugs herceptin and doxorubicin inhibit cardiac microvascular endothelial cell barrier formation resulting in increased drug permeability. *Biol. Open* **5**, 1362–1370 (2016).
6. A. Bielak-Zmijewska, M. Wnuk, D. Przybylska, W. Grabowska, A. Lewinska, O. Alster, Z. Korwek, A. Cmoch, A. Myszka, S. Pikula, G. Mosieniak, E. Sikora, A comparison of replicative senescence and doxorubicin-induced premature senescence of vascular smooth muscle cells isolated from human aorta. *Biogerontology* **15**, 47–64 (2014).
7. D. Cappetta, G. Esposito, E. Piegari, R. Russo, L. P. Ciuffreda, A. Rivellino, L. Berrino, F. Rossi, A. De Angelis, K. Urbanek, SIRT1 activation attenuates diastolic dysfunction by reducing cardiac fibrosis in a model of anthracycline cardiomyopathy. *Int. J. Cardiol.* **205**, 99–110 (2016).
8. H. Zhan, K. Aizawa, J. Sun, S. Tomida, K. Otsu, S. J. Conway, P. J. Mckinnon, I. Manabe, I. Komuro, K. Miyagawa, R. Nagai, T. Suzuki, Ataxia telangiectasia mutated in cardiac fibroblasts regulates doxorubicin-induced cardiotoxicity. *Cardiovasc. Res.* **110**, 85–95 (2016).
9. F. Aminkeng, A. P. Bhavsar, H. Visscher, S. R. Rassekh, Y. Li, J. W. Lee, L. R. Brunham, H. N. Caron, E. C. van Dalen, L. C. Kremer, H. J. van der Pal, U. Amstutz, M. J. Rieder, D. Bernstein, B. C. Carleton, M. R. Hayden, C. J. Ross; Canadian Pharmacogenomics Network for Drug Safety Consortium, A coding variant in RARG confers susceptibility to anthracycline-induced cardiotoxicity in childhood cancer. *Nat. Genet.* **47**, 1079–1084 (2015).
10. B. P. Schneider, F. Shen, L. Gardner, M. Radovich, L. Li, K. D. Miller, G. Jiang, D. Lai, A. O'Neill, J. A. Sparano, N. E. Davidson, D. Cameron, I. Gradus-Pizlo, R. A. Mastouri, T. M. Suter, T. Foroud, G. W. Sledge Jr., Genome-wide association study for anthracycline-induced congestive heart failure. *Clin. Cancer Res.* **23**, 43–51 (2017).
11. D. J. Serie, J. E. Crook, B. M. Necela, T. J. Dockter, X. Wang, Y. W. Asmann, D. Fairweather, K. A. Bruno, G. Colon-Otero, E. A. Perez, E. A. Thompson, N. Norton, Genome-wide association study of cardiotoxicity in the NCCTG N9831 (Alliance) adjuvant trastuzumab trial. *Pharmacogenet. Genomics* **27**, 378–385 (2017).
12. Y. Ding, X. Sun, W. Huang, T. Hoage, M. Redfield, S. Kushwaha, S. Sivasubbu, X. Lin, S. Ekker, X. Xu, Haploinsufficiency of target of rapamycin attenuates cardiomyopathies in adult zebrafish. *Circ. Res.* **109**, 658–669 (2011).
13. Y. Ding, P. A. Long, J. M. Bos, Y. H. Shih, X. Ma, R. S. Sundsbak, J. Chen, Y. Jiang, L. Zhao, X. Hu, J. Wang, Y. Shi, M. J. Ackerman, X. Lin, S. C. Ekker, M. M. Redfield, T. M. Olson, X. Xu, A modifier screen identifies DNAJB6 as a cardiomyopathy susceptibility gene. *JCI Insight* **1**, e88797 (2016).
14. K. J. Clark, D. Balciunas, H.-M. Pogoda, Y. Ding, S. E. Westcot, V. M. Bedell, T. M. Greenwood, M. D. Urban, K. J. Skuster, A. M. Petzold, J. Ni, A. L. Nielsen, A. Patowary, V. Scaria, S. Sivasubbu, X. Xu, M. Hammerschmidt, S. C. Ekker, In vivo protein trapping produces a functional expression codex of the vertebrate proteome. *Nat. Methods* **8**, 506–515 (2011).
15. L. Burg, N. Palmer, K. Kikhi, E. S. Miroshnik, H. Rueckert, E. Gaddy, C. MacPherson Cunningham, K. Mattonet, S.-L. Lai, R. Marín-Juez, R. B. Waring, D. Y. R. Stainier, D. Balciunas, Conditional mutagenesis by oligonucleotide-mediated integration of loxP sites in zebrafish. *PLOS Genet.* **14**, e1007754 (2018).
16. R. M. Evans, D. J. Mangelsdorf, Nuclear receptors, RXR, and the big bang. *Cell* **157**, 255–266 (2014).
17. H. M. Sucov, E. Dyson, C. L. Gumeringer, J. Price, K. R. Chien, R. M. Evans, RXR alpha mutant mice establish a genetic basis for vitamin A signaling in heart morphogenesis. *Genes Dev.* **8**, 1007–1018 (1994).
18. J. Chen, S. W. Kubalak, K. R. Chien, Ventricular muscle-restricted targeting of the RXRalpha gene reveals a non-cell-autonomous requirement in cardiac chamber morphogenesis. *Development* **125**, 1943–1949 (1998).
19. E. Merki, M. Zamora, A. Raya, Y. Kawakami, J. Wang, X. Zhang, J. Burch, S. W. Kubalak, P. Kaliman, J. C. I. Belmonte, K. R. Chien, P. Ruiz-Lozano, Epicardial retinoid X receptor α is required for myocardial growth and coronary artery formation. *Proc. Natl. Acad. Sci. U.S.A.* **102**, 18455–18460 (2005).
20. V. Subbarayan, M. Mark, N. Messadeq, P. Rustin, P. Chambon, P. Kastner, RXRα overexpression in cardiomyocytes causes dilated cardiomyopathy but fails to rescue myocardial hypoplasia in RXRα-null fetuses. *J. Clin. Invest.* **105**, 387–394 (2000).
21. C. M. Tran, H. M. Sucov, The RXRalpha gene functions in a non-cell-autonomous manner during mouse cardiac morphogenesis. *Development* **125**, 1951–1956 (1998).
22. J. C. Osorio, W. C. Stanley, A. Linke, M. Castellari, Q. N. Diep, A. R. Panchal, T. H. Hintze, G. D. Lopaschuk, F. A. Recchia, Impaired myocardial fatty acid oxidation and reduced

protein expression of retinoid X receptor-α in pacing-induced heart failure. *Circulation* **106**, 606–612 (2002).
23. R. S. Guleria, A. B. Singh, I. T. Nizamutdinova, T. Souslova, A. A. Mohammad, J. A. Kendall Jr., K. M. Baker, J. Pan, Activation of retinoid receptor-mediated signaling ameliorates diabetes-induced cardiac dysfunction in Zucker diabetic rats. *J. Mol. Cell. Cardiol.* **57**, 106–118 (2013).
24. S. J. Rasouli, D. Y. R. Stainier, Regulation of cardiomyocyte behavior in zebrafish trabeculation by Neuregulin 2a signaling. *Nat. Commun.* **8**, 15281 (2017).
25. H. Zhang, A. V. Dvornikov, I. G. Huttner, X. Ma, C. F. Santiago, D. Fatkin, X. Xu, A Langendorff-like system to quantify cardiac pump function in adult zebrafish. *Dis. Model. Mech.* **11**, dmm034819 (2018).
26. E. D'Aniello, A. B. Rydeen, J. L. Anderson, A. Mandal, J. S. Waxman, Depletion of retinoic acid receptors initiates a novel positive feedback mechanism that promotes teratogenic increases in retinoic acid. *PLOS Genet.* **9**, e1003689 (2013).
27. K. Kikuchi, V. Gupta, J. Wang, J. E. Holdway, A. A. Wills, Y. Fang, K. D. Poss, tcf21^{+} epicardial cells adopt non-myocardial fates during zebrafish heart development and regeneration. *Development* **138**, 2895–2902 (2011).
28. Y. Liu, A. Asnani, L. Zou, V. L. Bentley, M. Yu, Y. Wang, G. Dellaire, K. S. Sarkar, M. Dai, H. H. Chen, D. E. Sosnovik, J. T. Shin, D. A. Haber, J. N. Berman, W. Chao, R. T. Peterson, Visnagin protects against doxorubicin-induced cardiomyopathy through modulation of mitochondrial malate dehydrogenase. *Sci. Transl. Med.* **6**, 266ra170 (2014).
29. Y. Wallez, P. Huber, Endothelial adherens and tight junctions in vascular homeostasis, inflammation and angiogenesis. *Biochim. Biophys. Acta* **1778**, 794–809 (2008).
30. H. Kubota, H. Chiba, Y. Takakuwa, M. Osanai, H. Tobioka, G.-I. Kohama, M. Mori, N. Sawada, Retinoid X receptor α and retinoic acid receptor γ mediate expression of genes encoding tight-junction proteins and barrier function in F9 cells during visceral endodermal differentiation. *Exp. Cell Res.* **263**, 163–172 (2001).
31. M. R. Mizee, D. Wooldrik, K. A. M. Lakeman, B. van het Hof, J. A. R. Drexhage, D. Geerts, M. Bugiani, E. Aronica, R. E. Mebius, A. Prat, H. E. de Vries, A. Reijerkerk, Retinoic acid induces blood–brain barrier development. *J. Neurosci.* **33**, 1660–1671 (2013).
32. M. D. Zhou, H. M. Sucov, R. M. Evans, K. R. Chien, Retinoid-dependent pathways suppress myocardial cell hypertrophy. *Proc. Natl. Acad. Sci. U.S.A.* **92**, 7391–7395 (1995).
33. R. S. Guleria, R. Choudhary, T. Tanaka, K. M. Baker, J. Pan, Retinoic acid receptor-mediated signaling protects cardiomyocytes from hyperglycemia induced apoptosis: Role of the renin-angiotensin system. *J. Cell. Physiol.* **226**, 1292–1307 (2011).
34. P. W. Burridge, Y. F. Li, E. Matsa, H. Wu, S.-G. Ong, A. Sharma, A. Holmström, A. C. Chang, M. J. Coronado, A. D. Ebert, J. W. Knowles, M. L. Telli, R. M. Witteles, H. M. Blau, D. Bernstein, R. B. Altman, J. C. Wu, Human induced pluripotent stem cell–derived cardiomyocytes recapitulate the predilection of breast cancer patients to doxorubicin-induced cardiotoxicity. *Nat. Med.* **22**, 547–556 (2016).
35. M. Räsänen, J. Degerman, T. A. Nissinen, I. Miinalainen, R. Kerkelä, A. Siltanen, J. T. Backman, E. Mervaala, J. J. Hulmi, R. Kivelä, K. Alitalo, VEGF-B gene therapy inhibits doxorubicin-induced cardiotoxicity by endothelial protection. *Proc. Natl. Acad. Sci. U.S.A.* **113**, 13144–13149 (2016).
36. V. Achan, C. T. L. Tran, F. Arrigoni, G. S. Whitley, J. M. Leiper, P. Vallance, all-trans-Retinoic acid increases nitric oxide synthesis by endothelial cells: A role for the induction of dimethylarginine dimethylaminohydrolase. *Circ. Res.* **90**, 764–769 (2002).
37. B. L. Bohnsack, L. Lai, P. Dolle, K. K. Hirschi, Signaling hierarchy downstream of retinoic acid that independently regulates vascular remodeling and endothelial cell proliferation. *Genes Dev.* **18**, 1345–1358 (2004).
38. L. Lai, B. L. Bohnsack, K. Niederreither, K. K. Hirschi, Retinoic acid regulates endothelial cell proliferation during vasculogenesis. *Development* **130**, 6465–6474 (2003).
39. K. Kikuchi, J. E. Holdway, R. J. Major, N. Blum, R. D. Dahn, G. Begemann, K. D. Poss, Retinoic acid production by endocardium and epicardium is an injury response essential for zebrafish heart regeneration. *Dev. Cell* **20**, 397–404 (2011).
40. K. Pollinger, R. Hennig, A. Ohlmann, R. Fuchshofer, R. Wenzel, M. Breunig, J. Tessmar, E. R. Tamm, A. Goepferich, Ligand-functionalized nanoparticles target endothelial cells in retinal capillaries after systemic application. *Proc. Natl. Acad. Sci. U.S.A.* **110**, 6115–6120 (2013).
41. D. J. Lenihan, The horizon in cardio-oncology: "you are only as good as your endothelium". *J. Am. Coll. Cardiol.* **70**, 163–164 (2017).
42. R. C. Kane, W. D. McGuinn Jr., R. Dagher, R. Justice, R. Pazdur, Dexrazoxane (Totect^{TM}): FDA review and approval for the treatment of accidental extravasation following intravenous anthracycline chemotherapy. *Oncologist* **13**, 445–450 (2008).
43. L. Altucci, M. D. Leibowitz, K. M. Ogilvie, A. R. de Lera, H. Gronemeyer, RAR and RXR modulation in cancer and metabolic disease. *Nat. Rev. Drug Discov.* **6**, 793–810 (2007).
44. D. J. Straus, M. Duvic, S. M. Horwitz, K. Hymes, A. Goy, F. J. Hernandez-Ilizaliturri, T. Feldman, B. Wegner, P. L. Myskowski, Final results of phase II trial of doxorubicin HCl liposome injection followed by bexarotene in advanced cutaneous T-cell lymphoma. *Ann. Oncol.* **25**, 206–210 (2014).
45. L. W. Wang, I. G. Huttner, C. F. Santiago, S. H. Kesteven, Z.-Y. Yu, M. P. Feneley, D. Fatkin, Standardized echocardiographic assessment of cardiac function in normal adult zebrafish and heart disease models. *Dis. Model. Mech.* **10**, 63–76 (2017).

Acknowledgments: We thank K. Stragey and B. Gore for maintaining the zebrafish facility at the Mayo Clinic. We thank C. Burns, G. Burns, K. Poss, and ZIRC for generously sharing transgenic animals; M. Underhill for generously sharing RA-related plasmids; and J. Sun for generously granting us access to a flow cytometer in his laboratory. **Funding:** This work was supported in part by U.S. NIH R01 grants (HL81753 and HL107304 to X.X., HL111437 to T.K.H. and X.X., GM63904 to S.C.E. and X.X., and HG006431 to S.C.E.), the Mayo Foundation (to X.X. and S.C.E.), and a Scientist Development Grant from the American Heart Association (14SDG18160021 to Y.D.). This work was also made possible by CTSA grant UL1TR002377 from the National Center for Advancing Translational Sciences (NCATS), a component of the NIH.
Author contributions: X.M. and X.X. conceived the project, designed the experiments, interpreted the data, and drafted the original manuscript. X.M. performed experiments, collected the data, and generated figures. P.Z. performed in situ hybridization and immunostaining on adult zebrafish tissues. Y.D. contributed to the generation of transgenic animals. H.Z. and A.V.D. performed ex vivo cardiac pump assays. Q.Q. and M.L. evaluated the treatment of compounds and performed echocardiography on adult zebrafish. Z.W. performed the flow cytometry analysis. M.K. contributed to cell culture–related experiments. Y.W. evaluated the treatment of compounds in embryonic zebrafish. Y.Y. performed the R coding for heat map. N.N. analyzed GWAS-related data. X.X. supervised the research. J.H., S.C.E., T.K.H., and X.L. made critical intellectual contributions and edited the manuscript.
Competing interests: The authors declare that they have no competing interests. **Data and materials availability:** All data needed to evaluate the conclusions in the paper are present in the paper and/or the Supplementary Materials. Additional data that are presented as "data not shown" in the text may be requested from the authors. *rxraae2* and *Tg*(β*actin2:loxP-mCherry-stop-loxP-rxraa-EGFP*) also named *Tg*(β*act2:RSRxraa*) can be provided by X.X. pending scientific review and a completed material transfer agreement. Requests for these two lines should be submitted to X.X. (xu.xiaolei@mayo.edu).

Submitted 6 June 2019
Accepted 22 November 2019
Published 29 January 2020
10.1126/sciadv.aay2939

Citation: X. Ma, P. Zhu, Y. Ding, H. Zhang, Q. Qiu, A. V. Dvornikov, Z. Wang, M. Kim, Y. Wang, M. Lowerison, Y. Yu, N. Norton, J. Herrmann, S. C. Ekker, T. K. Hsiai, X. Lin, X. Xu, Retinoid X receptor alpha is a spatiotemporally predominant therapeutic target for anthracycline-induced cardiotoxicity. *Sci. Adv.* **6**, eaay2939 (2020).